ON THE ROLE OF HIGH LATITUDE ICE, SNOW, AND VEGETATION FEEDBACKS IN THE CLIMATIC RESPONSE TO EXTERNAL FORCING CHANGES

L. D. DANNY HARVEY
Department of Geography, University of Toronto, 100 St. George Street, Toronto, Canada, M5S 1A1

Abstract. A seasonal energy balance climate model containing a detailed treatment of surface and planetary albedo, and in which seasonally varying land snow and sea ice amounts are simulated in terms of a number of explicit physical processes, is used to investigate the role of high latitude ice, snow, and vegetation feedback processes. Feedback processes are quantified by computing changes in radiative forcing and feedback factors associated with individual processes. Global sea ice albedo feedback is 5–8 times stronger than global land snowcover albedo feedback for a 2% solar constant increase or decrease, with Southern Hemisphere cryosphere feedback being 2–5 times stronger than Northern Hemisphere cryosphere feedback.

In the absence of changes in ice extent, changes in ice thickness in response to an increase in solar constant are associated with an increase in summer surface melting which is exactly balanced by increased basal winter freezing, and a reduction in the upward ocean-air flux in summer which is exactly balanced by an increased flux in winter, with no change in the annual mean ocean-air flux. Changes in the mean annual ocean-air heat flux require changes in mean annual ice extent, and are constrained to equal the change in meridional oceanic heat flux convergence in equilibrium. Feedback between ice extent and the meridional oceanic heat flux obtained by scaling the oceanic heat diffusion coefficient by the ice-free fraction regulates the feedback between ice extent and mean annual air-sea heat fluxes in polar regions, and has a modest effect on model-simulated high latitude temperature change.

Accounting for the partial masking effect of vegetation on snow-covered land reduces the Northern Hemisphere mean temperature response to a 2% solar constant decrease or increase by 20% and 10%, respectively, even though the radiative forcing change caused by land snowcover changes is about 3 times larger in the absence of vegetational masking. Two parameterizations of the tundra fraction are tested: one based on mean annual land air temperature, and the other based on July land air temperature. The enhancement of the mean Northern Hemisphere temperature response to solar constant changes when the forest-tundra ecotone is allowed to shift with climate is only 1/3 to 1/2 that obtained by Otterman *et al.* (1984) when the mean annual parameterization is used here, and only 1/4 to 1/3 as large using the July parameterization.

The parameterized temperature dependence of ice and snow albedo is found to enhance the global mean temperature response to a 2% solar constant increase by only 0.04 °C, in sharp contrast to the results of Washington and Meehl (1986) obtained with a mean annual model. However, there are significant differences in the method used here and in Washington and Meehl to estimate the importance of this feedback process. When their approach is used in a mean annual version of the present model, closer agreement to their results is obtained.

Climatic Change **13** (1988) 191–224.

1. Introduction

Feedback processes involving snow and sea ice affect climatic sensitivity to external forcing changes in a number of distinct ways. Changes in land snow-cover area, albedo, or depth influence the effective mean albedo of snow-covered regions, while the albedo in zones with sea ice depends on the sea ice fraction, albedo of bare sea ice, and the thickness and albedo of any snow present on the ice. As well, sea ice has a dramatic influence on air-sea heat fluxes, which may change either in response to a change in ice extent or in the thickness of the ice itself. It has also been suggested that changes in sea ice extent may influence high latitude temperatures by altering meridional heat transport by ocean currents. Also of potential importance are possible feedbacks between snow and ice cover and cloudiness.

In this paper an Energy Balance Climate Model (EBCM) which simulates zonal ice and snow fractions in terms of a number of explicit physical processes is used to investigate snow and ice feedback processes and their interactive effect with other model feedback processes. In particular, this paper addresses five interconnected issues: (1) resolution of the conflicting explanations given by Manabe and Stouffer (1980) and Robock (1983) for the greater high-latitude temperature sensitivity in winter rather than summer as indicated by their climate models; (2) the importance of feedback between sea ice fraction and the oceanic meridional heat flux diffusion coefficient; (3) the relative contributions of sea ice and land snow feedbacks on a hemispheric basis and in the global mean; (4) the importance of partial vegetational masking of snowcover and of shifts in the tundra-forest ecotone; and (5) the effect on model sensitivity to external forcing changes of temperature dependencies for ice and snow albedos. Feedback processes are quantified and compared with those of other climate models by calculating both radiative damping parameters and feedback factors for individual processes.

2. Model Description

The atmospheric and land surface components of the EBCM used here are described in Harvey (1988a), while the sea ice component is described in Harvey (1988b); thus, only a brief description is given here. The model is illustrated for the reader's convenience in Figure 1. The model has latitudinal, surface-air, and land-sea resolution, and is forced with seasonally varying insolation. Here, 2.5° latitudinal resolution is used between 80–40° N and 75–40° S, where fluctuating ice and snow limits occur, with 5°–10° resolution outside these latitudes. In computing solar radiative transfer, account is taken of O_3 absorption, Rayleigh scattering, tropospheric aerosols, cloud droplet absorption and scattering, and water vapor absorption. Radiative fluxes are computed separately in the visible and near infrared (NIR) parts of the spectrum, the distinction between direct and

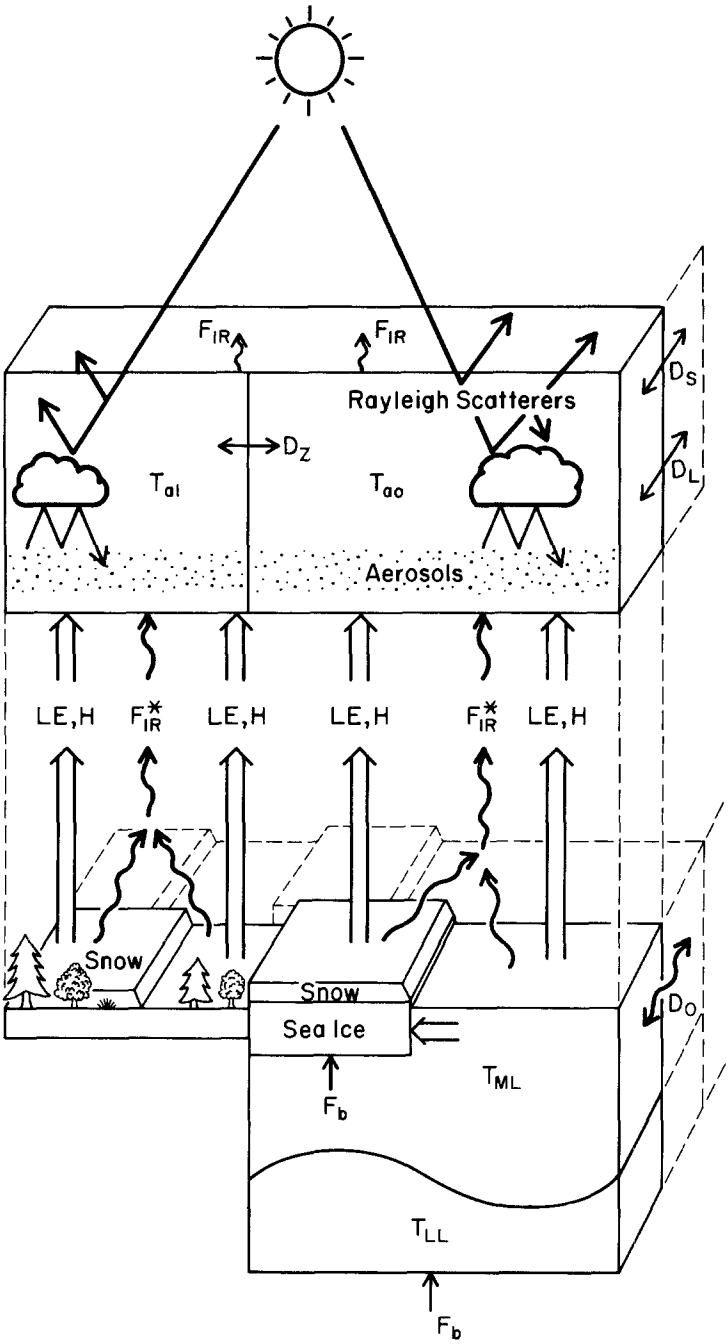

Fig. 1. Schematic illustration of one zone from the model used here, containing land, ocean, and partial snow and sea ice cover. H and LE are the vertical turbulent fluxes of sensible and latent heat, F_{IR} refers to infrared radiation, F_b is the upward heat flux at the base of sea ice and the mixed layer, D_Z is a coefficient for east-west heat exchange, and D_H, D_L, and D_O are diffusion coefficients for meridional fluxes of atmospheric sensible, atmospheric latent, and oceanic sensible heat.

diffuse beam radiation is retained throughout the calculations, and the zenith angle dependent Delta-Eddington formulation is used for cloud and aerosol layers. Simple parameterizations are used to compute infrared fluxes, while the vertical fluxes of latent and sensible heat are computed using bulk aerodynamic formulae with exchange coefficients which depend on the surface-air temperature difference. Meridional atmospheric sensible, atmospheric latent, and oceanic heat fluxes are separately parameterized as diffusion.

Observed precipitation rates are used but uniformly scaled so that global precipitation equals global evaporation on each time step. The fraction of a grid box over which precipitation falls as snow is parameterized as a function of air temperature; as seasonal temperatures decrease the portion of land grid boxes covered with snow gradually increases. Snowmelt is computed based on the surface energy balance, and is partitioned between a decrease in snow extent and a decrease in snow depth, so that snow area gradually decreases during the spring snowmelt period.

In zones with partial land snow cover, separate land surface temperatures, albedos, and energy balances are computed for the snow-covered and snow-free parts of the zone. Separate surface albedos are computed in the visible and NIR parts of the spectrum and for direct and diffuse beam radiation. Snow-free land surface albedos are computed based on the fraction of a given land zone covered in each of ten different vegetation (and associated soil) categories, and the fraction of each category seen as foliage and as soil. Vegetation types, vegetation and soil spectral albedos, and winter and summer foliage fractions are given in Briegleb and Ramanathan (1982) (henceforth referred to as BR). Zonally-averaged fractions for each vegetation type were computed from the input data used for the NCAR Community Climate Model (CCM), which is reference BR. In the snow-covered part of the zone the mean albedo is given by the vegetation and snow albedos weighted by the effective snow-cover fraction f, which, for vegetation type i, is given by

$$f_{si} = h_s/(h_s + R_i), \tag{1}$$

where h_s is the water equivalent snow depth and R_i is the roughness of vegetation type i. This parameterization was used by BR, where values of R_i may be found. The most important differences are between non-forest and forest vegetation categories, with R_i ranging from 0.01 to 0.03 m for the former, and from 0.3 to 0.5 m for extratropical forests. The f_{si} are weighted by the corresponding vegetation fractions to get the mean effective snow-cover fraction f_s for the snowcovered region, which is then used to compute the mean albedo of the snowcovered part of the zone as

$$\alpha_{sc}(\theta) = f_s \alpha_{\text{snow}}(\theta) + (1 - f_s)\alpha_{\text{veg}}(\theta) \tag{2}$$

where $\alpha_{\text{veg}}(\theta)$ is the zonal mean vegetation albedo, and θ is zenith angle. For later use in analyzing model results, the zonal fraction of tundra + no vegetation,

TABLE I: Fraction of land zones assigned to tundra + polar desert, other non-forest vegetation classes, and forest. Also given is the zonal mean vegetation roughness R.

Latitude	Tundra + polar desert	Other non-forest vegetation	Forest vegetation	R(m)
85–90° N	1.000	0.000	0.000	0.01
80–85° N	1.000	0.000	0.000	0.01
75–80° N	1.000	0.000	0.000	0.01
70–75° N	1.000	0.000	0.000	0.01
65–70° N	0.586	0.000	0.414	0.23
60–65° N	0.334	0.059	0.607	0.31
55–60° N	0.105	0.263	0.632	0.31
50–55° N	0.023	0.563	0.409	0.22
45–50° N	0.000	0.725	0.275	0.15
40–45° N	0.000	0.909	0.091	0.07

other non-forest vegetation categories, and total forest fraction, as well as the zonal mean vegetation roughness, are given in Table I for the 40°–90° N region. The snow albedo appearing in Equation (2) is itself a function of snow temperature and age, as well as depending on zenith angle.

The sea ice model predicts zonal mean fractional ice cover, ice thickness, and snow depth (if snow is present). Vertical ice growth or decay rates are computed using the zero layer model of Semtner (1976), with minor modifications described in Harvey (1988b). Ice fraction is computed based on an analytic solution of the ice growth equations of Hibler (1979), which permits ice fraction to continuously increase or decrease and permits partial ice cover within a given ocean grid box. When partial ice cover occurs, separate temperatures are computed for the sub-ice and lead mixed layer water, neither of which is constrained to be at the freezing point of sea water when ice is present in a zone (although neither is permitted to fall below the freezing point of sea water). Growth of new ice in leads or lateral melting of existing ice from leads may occur. A fixed upward heat flux of 2 W m^{-2} in the Northern Hemisphere and 15–30 W m^{-2} in the Southern Hemisphere is applied at the ice base and at the base of the ice-free mixed layer in polar regions, which is compensated by a downward heat flux out of the mixed layer in tropical regions. These fluxes represent the effect of the thermohaline circulation and have been found to be necessary for the realistic simulation of sea ice in the present as well as in other sea ice models (i.e.: Parkinson and Washington, 1979). A meridional advection of ice is prescribed which opens up new leads and extends the equatorward ice limit.

The albedo of sea ice depends on the ice temperature, varying linearly from a maximum value at −3 °C to a minimum value at 0 °C. Snow may occur on sea ice, in which case its albedo is computed in the same way as for snow on land in the absence of vegetation, as explained in Harvey (1988a). The combined ice-snow albedo is given by

TABLE II: Lower and upper spectral albedos for snow and sea ice. The albedo values given here are diffuse beam albedo; a zenith angle correction is added to get direct beam albedos.

		Visible	Near infrared
Sea ice,	Lower	0.50	0.08
	Upper	0.65	0.38
Snow,	Lower	0.76	0.33
	Upper	0.82	0.62

$$\alpha_{is}(\theta) = \begin{cases} \alpha_{ice}(\theta) + (\alpha_{snow}(\theta) - \alpha_{ice}(\theta))\ 100\ h_s & h_s < 0.01 \\ \alpha_{snow}(\theta) & h_s \geqslant 0.01. \end{cases} \quad (3)$$

Lower and upper limits of the spectral sea ice and snow albedos used here are given in Table II; the values given in Table II pertain to diffuse beam radiation, and are modified for direct beam radiation as explained in Harvey (1988a) to account for zenith angle effects.

In the base case version of the model land vegetation fractions are fixed. Snow on forest has a considerably smaller effective snowcover fraction than snow of the same depth on tundra, leading to a smaller albedo for the snow-covered part of the zone when forest is present in place of tundra. Otterman *et al.* (1984; henceforth referred to as OCA) investigated the importance to climate sensitivity of the lower effective snow albedo on forest and of shifts in the treeline using a mean annual model. To investigate the potential role of shifts in the tundra-forest ecotone in the present model, sensitivity experiments are performed in which the fraction of tundra or polar desert is parameterized either in terms of mean annual land air temperature as

$$f_{tundra} = \begin{cases} 1.0 & T \leqslant 260\ \text{K} \\ (274 - T)/14 & 260\ \text{K} < T < 274\ \text{K} \\ 0.0 & T \geqslant 274\ \text{K} \end{cases} \quad (4)$$

or in terms of July land air temperature as

$$f_{tundra} = \begin{cases} 1.0 & T \leqslant 278\ \text{K} \\ (290 - T)/12 & 278\ \text{K} < T < 290\ \text{K} \\ 0.0 & T \geqslant 290\ \text{K} \end{cases} \quad (5)$$

These parameterizations were derived by correlating the zonal mean tundra + polar desert fractions given in Table I with zonally averaged land surface air temperatures obtained from Crutcher and Meserve (1970). These parameterizations give 50% tundra at a mean annual temperature of −6 °C if the first is used, or at a July temperature of 11 °C if the second is used. The first para-

meterization is comparable to that used by OCA, in which it is assumed that all vegetation poleward of the −5 °C mean annual isotherm is tundra. The second parameterization is consistent with the observed correlation of the treeline with the July 10 °C isotherm, which is evident upon comparing Figures 3 and 5 of Hare and Hay (1974). Since high latitude temperature sensitivity to solar constant or CO_2 changes in this and most other climate models is smaller for July than in the annual mean, one may expect the second parameterization to give smaller treeline shifts in response to these external forcing changes than would the parameterization based on mean annual temperature.

3. Linear Feedback Analysis Methodology

Several different parameters have been used in the climate modeling literature to represent the strengths of individual and collective climatic feedback processes. One of these is λ, which is given by

$$\lambda = \mathrm{d}F/\mathrm{d}T + Q_s \, \mathrm{d}\alpha_p/\mathrm{d}T, \tag{6}$$

where F is the global mean infrared emission to space, Q_s is the solar constant divided by 4, α_p is the global mean planetary albedo, and T is global mean temperature. The parameter λ is the rate at which the global mean net radiation changes as temperature changes, and is thus referred to as a radiative damping parameter. It has been extensively used to quantify and compare climate model sensitivities (i.e.: Dickinson *et al.*, 1987). If ΔT is the equilibrium global mean temperature response to an external forcing change ΔQ, then

$$\Delta T = \Delta Q/\lambda \tag{7}$$

which can be solved for λ.

In the absence of internal feedbacks other than through the explicit dependence of net radiation on temperature, we can write

$$\Delta T_0 = G_0 \Delta Q, \tag{8}$$

where G_0 is the climate system gain in the absence of feedbacks involving the implicit dependence of net radiation on T. As discussed in Schlesinger (1985), $G_0 = (\partial N/\partial T)^{-1}$, where N = global net radiation. The term $\partial N/\partial T$ is equivalent to $\partial F/\partial T$, so G_0 involves only the feedback between temperature and infrared radiation as given by the Planck function. In the present model $\partial F/\partial T$ and hence G_0 cannot be directly computed because infrared emission to space is computed using the parameterization of Thompson and Warren (1982), which incorporates the effect on infrared emission of concurrent changes in absolute humidity as temperature changes. However, Manabe and Wetherald (1967) showed that $\partial F/\partial T$ can be accurately estimated as the derivative of the spectrally integrated Planck function evaluated at the effective planetary radiating temperature. That is,

$$\partial F/\partial T = 4\sigma T_{\text{eff}}^3$$

where $T_{\text{eff}} = (F/\sigma)^{0.25}$ and σ is the Stefan-Boltzmann constant.

With implicit feedbacks we can write

$$\Delta T = G_0 (\Delta Q + \Delta J), \tag{9}$$

where ΔJ is the change in net radiation attributable to all implicit internal feedback processes. ΔJ itself depends on ΔT and involves a number of separate internal processes. That is, $\Delta J = \Sigma \Delta J_i = \Sigma l_i \Delta T = K \Delta T$. Letting $f = G_0 K$, we obtain

$$\Delta T = \frac{G_0}{1-f} \Delta Q. \tag{10}$$

The parameter f is referred to as a feedback factor by Schlesinger and Mitchell (1985) and Schlesinger (1985). From Equations (8) and (10) one obtains

$$f = 1 - \frac{\Delta T_0}{\Delta T}, \tag{11}$$

where ΔT_0 is the equilibrium temperature change in the absence of implicit feedback processes, and ΔT is the equilibrium temperature change in their presence.

It is generally assumed that f (and λ) is independent of the magnitude of the external forcing change ΔQ for small ΔQ, so that the global mean temperature response varies linearly with ΔQ. Furthermore, it is generally assumed that the contributions to f and λ from individual feedback processes combine linearly, so that $f = \Sigma f_i$ and $\lambda = \lambda_0 + \Sigma \lambda_i$, where $\lambda_0 = G_0^{-1}$ is the λ computed in the absence of implicit feedbacks. These assumptions are a corollary of the assumption that $\Delta J = \Sigma \Delta J_i$. It is also assumed that the individual f_i and λ_i for any given process are independent of whatever other processes may be present, altough the change in temperature response associated with the addition of any given feedback process does depend on what other feedback processes are already present, as may be seen from Equation (10). Thus, one approach in estimating the f_i or λ_i for individual feedback processes would be to compute the total f or λ for experiments with and without feedback process i operating, and take the difference.

Alternatively, it follows from the above that the f_i and λ_i can also be computed as

$$f_i = G_0 \Delta J_i / \Delta T \tag{12}$$

$$\lambda_i = -\Delta J_i / \Delta T, \tag{13}$$

where ΔJ_i is the change in net radiation at equilibrium caused by feedback process i acting alone. Note that the λ_i will be negative for positive feedback, whereas the f_i will be positive. To calculate the ΔJ_i, the values of temperature,

snow, and sea ice variables on each time step obtained in equilibrium for the present and altered solar constant are stored. For each ΔJ_i desired, a single year is simulated using the original solar constant, the new values of variable i, and the old values of all the other variables, and the change in net radiation determined. Using this approach, the f_i or λ_i associated with all the internal feedback processes can be computed from a single experiment in which all feedback processes are operative, rather than having to perform a series of experiments in which the various feedback processes are removed one at a time. Furthermore, the separate contributions to the global mean ΔJ_i from the Northern and Southern hemispheres can be used to determine the relative importance of feedback processes (such as those involving ice and snow) in the two hemispheres.

Finally, the direct contribution to the global mean temperature response from feedback process i can be computed as

$$\Delta T_i = G_0 \, \Delta J_i \tag{14}$$

which follows directly from Equation (9). The reader may consult Schlesinger (1985) for further discussion and examples of the linear feedback analysis methodology adopted here.

4. Results

As shown in Harvey (1988a), the model used here realistically simulates the seasonal variation of sea ice and land snow area in both hemispheres with present external forcing, although Southern Hemisphere sea ice extent tends to be slightly too large and Northern Hemisphere sea ice extent slightly too small. Since climate model sensitivity to external forcing changes is known to depend significantly on the initial ice and snow areas (Spelman and Manabe, 1984), the present model satisfies at least one of the necessary conditions for accurately estimating climate sensitivity, and can be used to study the role of ice and snow feedback processes.

4.1. *Base Case*

The latitude-month distribution of equilibrium land and sea atmospheric temperature response to a 2% solar constant increase is shown in Figure 2. These results can be compared with the corresponding temperature response shown in Figure 16 of Manabe and Stouffer (1980; henceforth referred to as MS), obtained for a CO_2 quadrupling in a General Circulation Model (GCM) having realistic geography, if their temperature responses are reduced roughly in half to account for the difference in external forcing change used here and in MS. The results obtained here are similar to those of MS in several important respects; in particular, there is a strong seasonal variation in temperature

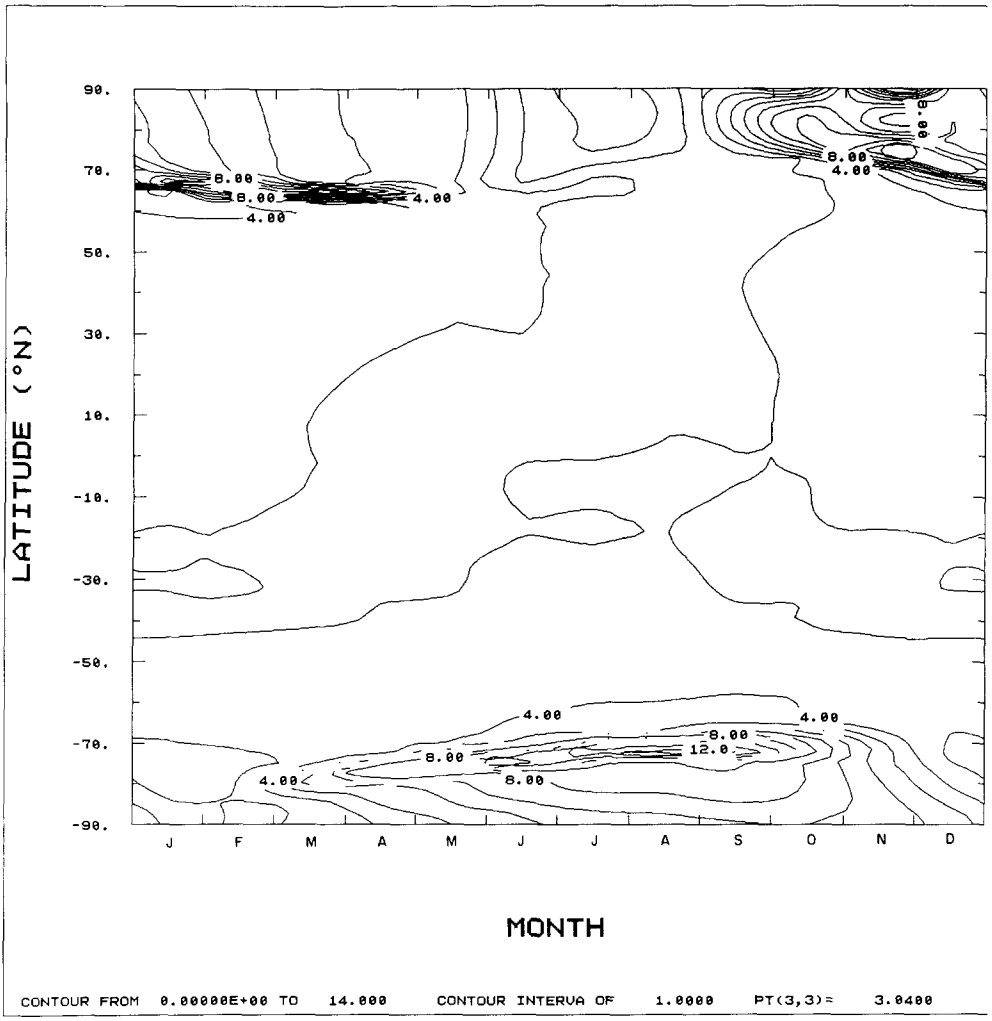

Fig. 2. Latitude-month response to a 2% solar constant increase of (a) oceanic air temperature, and (b) land air temperature.

response at high latitudes for both models, with maximum ocean air warming in early winter but progressively later with decreasing latitude, and maximum land air warming also in early winter but with a secondary maximum near 60° N in spring. In both models winter atmospheric temperature sensitivity is about 30% greater over the ocean than over the land, which indicates that land winter temperatures are largely responding to oceanic feedback processes. Finally, in both models there is very little seasonal variation of sensitivity in low latitudes.

The zonally averaged, mean annual atmospheric temperature responses for both a 2% solar constant increase and a 2 % solar constant decrease are shown in Figure 3, while Figure 4 shows the changes in Northern and Southern Hemi-

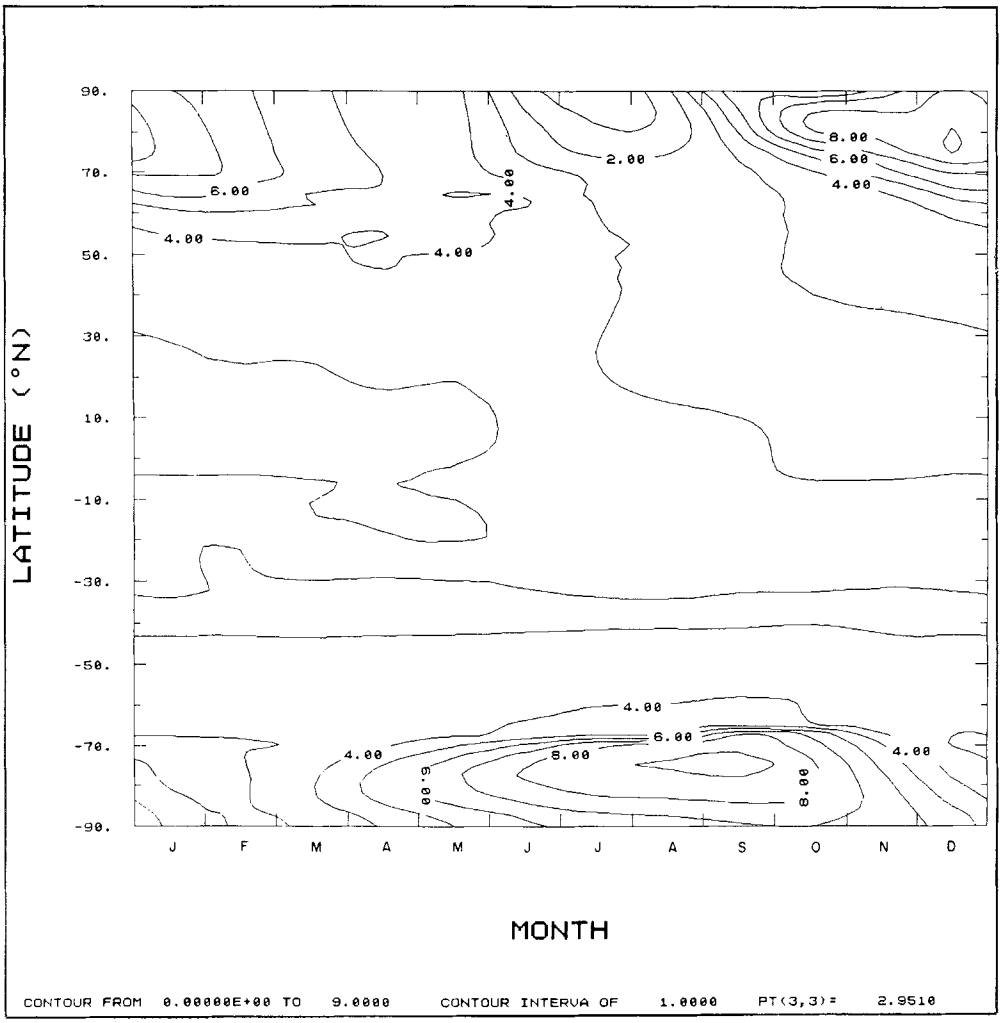

Fig. 2b.

sphere sea ice area and Northern Hemisphere land snow area (snow area does not change significantly in the Southern Hemisphere). The maximum high-latitude temperature sensitivity in the Southern Hemisphere is about 40% greater than that of the Northern Hemisphere for a solar constant increase and about 60% greater for a solar constant decrease. As seen from Figure 4, the change in Northern Hemisphere sea ice is comparable for a solar constant increase or decrease, whereas the seasonal change in Southern Hemisphere sea ice area is up to twice as large for a solar constant decrease as for an increase. This difference is a result of hemispheric differences in the land-sea geography. In the case of the Southern Hemisphere, the sea ice advances into zones where

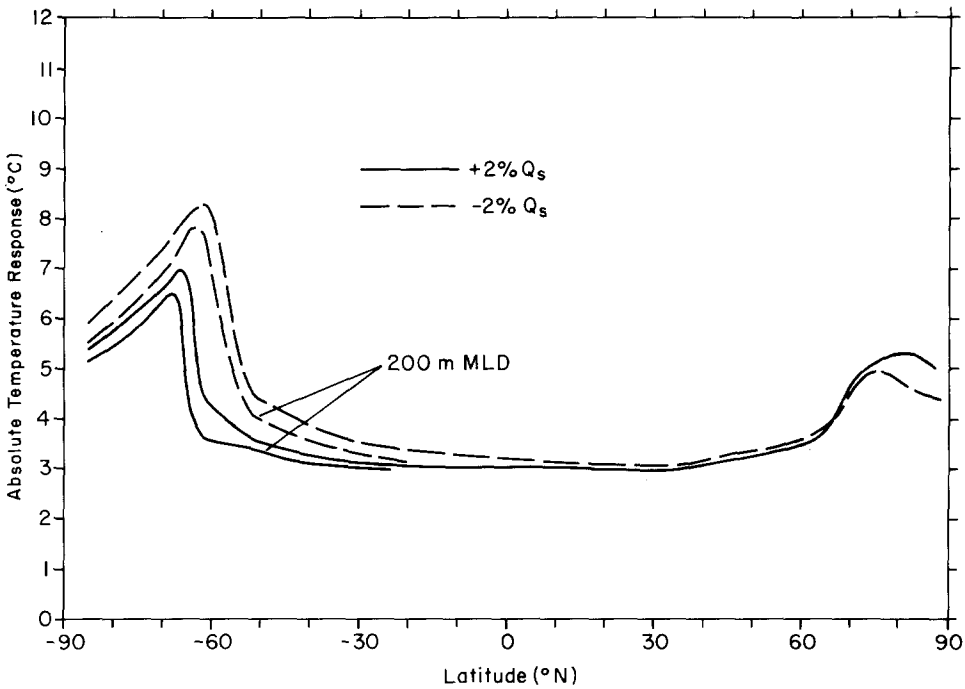

Fig. 3. Absolute values of mean annual, zonally averaged atmospheric temperature response to a 2% solar constant decrease and a 2% solar constant increase. Also shown is the high latitude Southern Hemisphere temperature response if a 200 m rather than a 100 m mixed layer depth is used poleward of 55° S.

the ocean fraction is close to 1.0 when the solar constant decreases, whereas sea ice retreats from zones where the ocean fraction and zonal area are smaller when the solar constant increases, resulting in a larger change in hemispheric ice area when the solar constant decreases. In the case of the Northern Hemisphere, the land-sea geography is such that comparable changes in hemispheric ice area occur when the solar constant increases or decreases by 2%.

As shown in Harvey (1988a, b), the extent of Southern Hemisphere sea ice is sensitive to the choice of mixed layer depth at high latitudes in the Southern Hemisphere, with winter ice being less extensive with a larger mixed layer depth. For this reason the above two experiments were also run using an ice-free mixed layer depth of 200 m rather than 100 m poleward of 55° S. Not surprisingly, this results in a smaller Southern Hemisphere climate sensitivity for both a solar constant decrease and increase (Figure 3), but still greater than in the Northern Hemisphere.

Estimation of Feedback Factors

Table III shows the ΔJ_i computed for the present model for both a 2% solar constant decrease and a 2% solar constant increase, as well as radiative damping

TABLE III: Changes in net radiation (ΔJ_i), radiative damping coefficients (λ_i), and feedback factors (f_i) associated with individual feedback processes for a 2% solar constant decrease and a 2% solar constant increase. Also given are the contributions to global mean air temperature change (ΔT_i) from individual feedback processes and from the original external forcing change. The terms in parenthesis in the ΔJ_i column are other energy terms which sum along with the ΔJ_i. See text for further explanation.

	ΔJ_i	λ_i	f_i	ΔT_i
(A) −2% Q_s: G_0	$= 0.2664$ (W m^{-2} °C^{-1})$^{-1}$			
ΔT	$= -3.745$ °C			
dF/dT	$= 1.98$ W m^{-2} °C^{-1}			
surface α	−1.864	−0.498	0.133	−0.497
H_2O-IR	−6.628	−1.770	0.472	−1.766
H_2O-α_p	−0.736	−0.197	0.052	−0.196
$-(\partial F/\partial T)\Delta T$	(14.057)	3.754	–	–
ΔQ	(−4.858)	–	–	−1.294
Sum	−0.029	1.289	0.657	−3.753
(B) +2% Q_s: G_0	$= 0.2607$ (W m^{-2} °C^{-1})$^{-1}$			
ΔT	$= 3.371$ °C			
dF/dT	$= 1.95$ W m^{-2} °C^{-1}			
surface α	1.064	−0.316	0.082	0.278
H_2O-IR	6.358	−1.886	0.492	1.658
H_2O-α_p	0.687	−0.204	0.053	0.179
$-(\partial F/\partial T)\Delta T$	(−12.931)	3.836	–	–
ΔQ	(4.858)	–	–	1.266
Sum	0.036	1.430	0.627	3.381

coefficients λ_i, feedback factors f_i, and the corresponding contribution ΔT_i to the total temperature response. Also given is G_0, dF/dT, and the actual ΔT. The individual ΔT_i would sum exactly to ΔT if the model were in exact equilibrium and if the ΔJ_i combined exactly linearly; as seen from Table III, the difference between $\Sigma \Delta T_i$ and ΔT is negligible. The term dF/dT is equivalent to the parameter B used in simple EBCM's, for which Short *et al.* (1984) recommend a value of 1.93 W m^{-2} °C^{-1}, in excellent agreement with the values given in Table III. Changes in absolute humidity influence the net energy balance in the infrared (identified as H_2O-IR in Table III) and in the solar (identified as H_2O-α_p) parts of the spectrum. The term $(\partial F/\partial T)\Delta T$ is the change in infrared emission to space which would occur in the absence of water vapor feedback. The infrared parameterization used here gives the change in F caused by changes in temperature and absolute humidity acting together, so that only the sum $\Delta J_{\text{H20-IR}} - (\partial F/\partial T)\Delta T$ can be directly computed here, but $\partial F/\partial T$ can be separately estimated as explained in Section 3. The terms in parenthesis in the ΔJ_i column are not ΔJ_i but should sum, along with the ΔJ_i, to zero; as seen from Table III, the residuals are negligible.

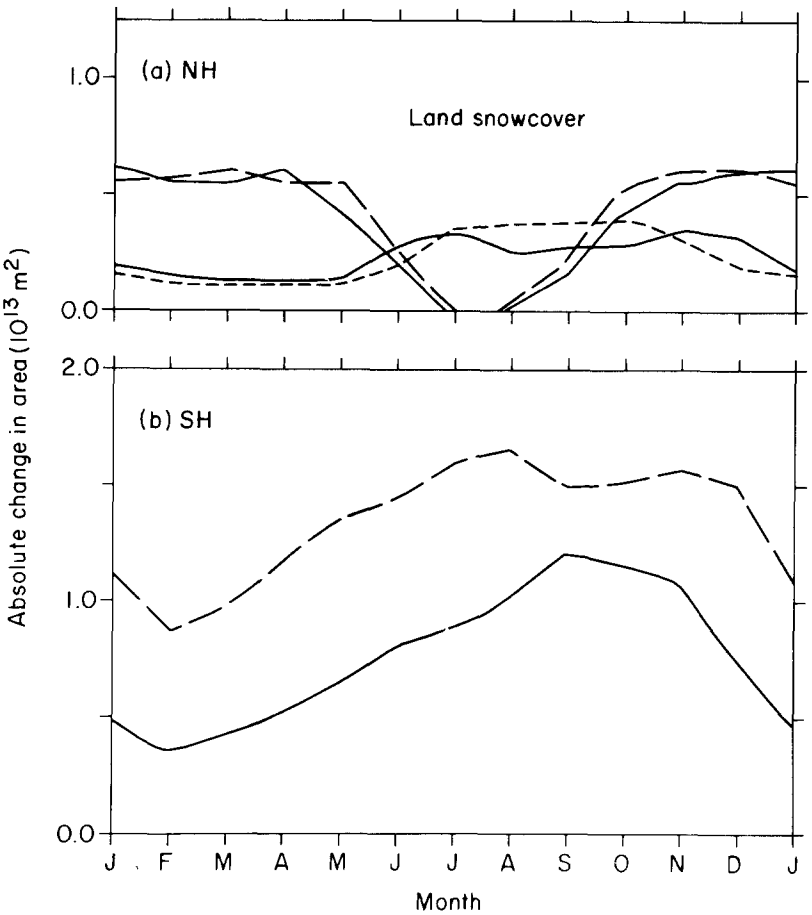

Fig. 4. Absolute values of change in hemispheric land snow and sea ice areas for a 2% solar constant decrease (dashed lines) and a 2% solar constant increase (solid lines).

It can be seen from Table III that the H_2O-infrared feedback is by far the strongest model feedback. The ice and snow surface albedo feedbacks together are only 1/6 as strong for a 2% solar constant increase, and only 1/4 as strong for a 2% solar constant decrease. The H_2O-solar feedback is also important, being about 60% as strong as the surface albedo feedbacks for a solar constant increase. As seen from Table III, ice and snow feedbacks contribute a global mean cooling of 0.5 °C for a 2% solar constant decrease (about 13% of the total response), and a global mean warming of 0.3 °C for a 2% solar constant increase (about 8% of the total response). Thus, the ice and snow feedbacks are comparatively weak in the global mean.

These temperature contributions, however, are only the direct contributions from ice and snow changes, and should not be confused with the change in model response which would occur if the ice and snow feedbacks were sup-

TABLE IV: Comparison of radiative damping coefficients λ (W m^{-2} °C^{-1}) and feedback factors f as computed for various models for $2 \times CO_2$ or a 1 or 2% solar constant increase. For simplicity, it is assumed that $G_0 = 0.26$ (W m^{-2} °C^{-1})$^{-1}$ for all models.

Model	Reference	$\lambda_{\alpha s}$	$\lambda_{H2O\text{-}\alpha p}$	$f_{\alpha s}$	$f_{H2O\text{-}\alpha p}$
GISS GCM	Hansen *et al.* (1984)	–0.35	–	0.09	–
OSU GCM	Schlesinger (1985)	–0.7	–	0.18	–
NCAR CCM	Dickinson *et al.* (1987)	–0.7	–0.2	0.18	0.05
EBCM	Robock (1983)	–0.67	–	0.17	–
Present Model		–0.32	–0.2	0.08	0.05

pressed. Since all of the ΔJ_i depend on the total model response ΔT, removal of any one feedback process not only removes the corresponding ΔJ_i, but also leads to a reduction in all the other ΔJ_i. To the extent that the model behaves linearly, however, the f_i and λ_i for the remaining processes will be unchanged. Equation (10) can thus be used along with the total f and $f_{\text{surface-}\alpha}$ given in Table III to compute globally averaged temperature responses of –2.72 °C and 2.78 °C for a 2% solar constant decrease and increase, respectively, in the absence of ice and snow feedbacks. The net effect of the ice and snow feedbacks is thus to enhance the cooling by 1.0 °C for a 2% solar constant decrease, and to enhance the warming by 0.6 °C for a 2% solar constant increase. Both of these enhancements are about twice the direct radiative effects indicated in Table III.

Table IV compares $\lambda_{\alpha s}$, $\lambda_{H2O\text{-}\alpha p}$, and the corresponding feedback factors as computed by the present and various other models. The present model agrees best with the GISS GCM for surface albedo feedback, but has a surface albedo feedback only half as strong as obtained by the OSU or NCAR models, or by Robock's (1983) EBCM. The H_2O-solar feedback agrees with the value ascribed to the NCAR CCM by Dickinson *et al.* (1987).

Table V gives the separate contributions of ice and snow changes in both

TABLE V: Breakdown of surface albedo contributions to the global mean ΔJ (W m^{-2}) for land snow and sea ice, and for the Northern Hemisphere (NH) and Southern Hemisphere (SH).

		–2% Q_s	+2% Q_s
Land snow:	NH	–0.196	0.163
	SH	–0.015	0.017
	Global	–0.211	0.180
Sea ice:	NH	–0.153	0.139
	SH	–1.499	0.745
	Global	–1.652	0.884
Ice + Snow:	NH	–0.349	0.302
	SH	–1.514	0.762
	Global	–1.863	1.064

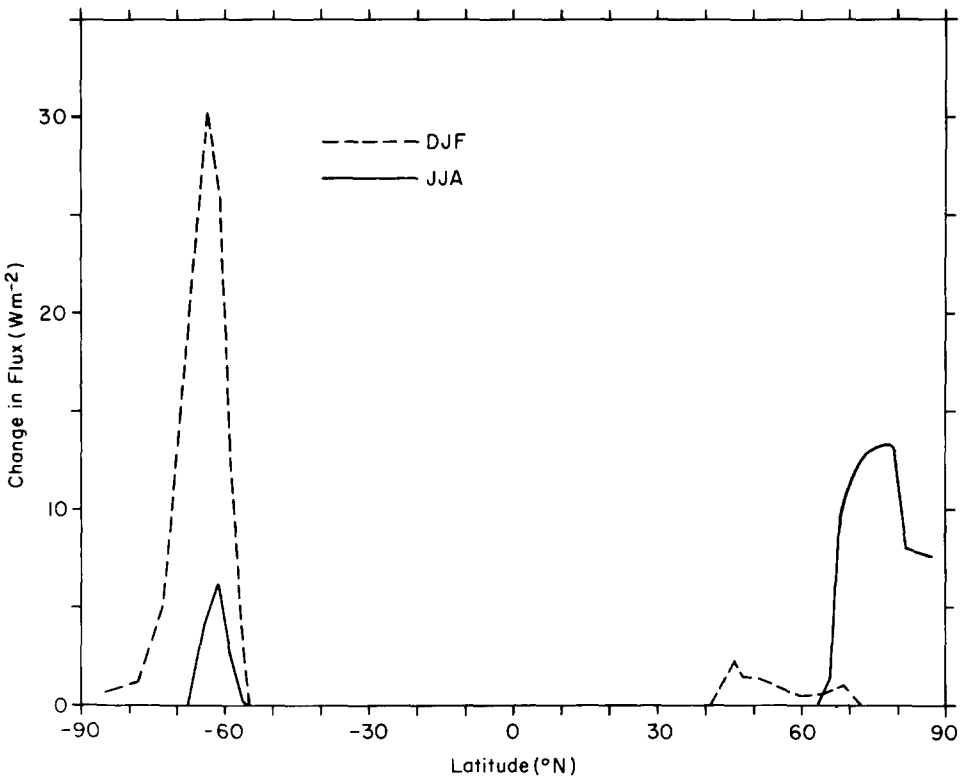

Fig. 5. Change in zonally averaged absorbed solar radiation caused by snow cover and ice changes for December-January-February (DJF) and June-July-August (JJA) for a 2% solar constant increase.

hemispheres to the global ΔJ, and it is readily seen that sea ice feedback dominates land snow cover feedback in both hemispheres, and that Southern Hemisphere cryosphere feedback (which is almost entirely a sea ice feedback) dominates Northern Hemisphere cryosphere feedback. Figure 5 shows the zonally averaged change in solar radiation caused by snow and ice for December–January–February (DJF) and June–July–August (JJA), and can be compared with the NCAR CCM results given in Figure 1 of Dickinson *et al.* (1987) for a CO_2 doubling.[1] The present model agrees well with the NCAR CCM at high Northern Hemisphere latitudes, but has a Southern Hemisphere high latitude change which is less than one-third of that obtained by Dickinson *et al.* (1987). Thus, although Southern Hemisphere sea ice feedback dominates the global land + snow feedback in the present model, it dominates by less than in the NCAR CCM. Dickinson *et al.* (1987) suggest that the Southern Hemisphere sea ice feedback is probably too strong in the version of the NCAR

[1] The results shown in Dickinson *et al.* (1987) also include the effect on solar radiation of water vapor and cloud changes, but at high latitudes the dominant effect is that of surface albedo changes.

CCM which they analyzed because too much Southern Hemisphere sea ice is simulated for the present external forcing.

The much greater sensitivity of the Southern Hemisphere than the Northern Hemisphere to a solar constant decrease raises interesting questions concerning Milankovitch orbital forcing changes and the origin of ice ages. Milankovitch (1941) had argued that summer insolation changes near 65° N drive ice ages, with low summer insolation at this latitude favoring growth of Northern Hemisphere ice sheets. A number of zero-dimensional ice age models have used summer insolation forcing at this latitude as the input forcing (i.e.: Imbrie and Imbrie, 1980). Since the effect on insolation of precessional orbital changes is out of phase in the two hemispheres, whereas temperature changes are largely in phase and follow the summer 65° N insolation changes (see Mercer, 1984), it has been further argued that high latitude feedback processes must have been stronger in the Northern Hemisphere and controlled the Southern Hemisphere response. This argument has been partly based on the larger high latitude land fraction in the Northern Hemisphere and the assumption that land snow cover feedbacks are more important to climate sensitivity than sea ice feedbacks. Pollard (1983), in trying to model the climatic response to Milankovitch insolation variations, neglected sea ice changes altogether, presumably on the grounds that sea ice feedbacks would be less important than land snow and ice feedbacks. However, sea ice feedback processes dominate land snow cover feedbacks in the present model and lead to greater Southern Hemisphere than Northern Hemisphere sensitivity when cooling occurs. The results obtained here thus raise serious questions concerning widely held assumptions regarding the relative importance of land versus snow and Northern Hemisphere versus Southern Hemisphere cryosphere feedbacks. These issues are explored further in Harvey (1988c).

4.2. *Role of Ice Thickness and Area Changes*

MS explained the greater high latitude atmospheric temperature sensitivity for their model in winter than in summer as a result of the additional heating following a CO_2 increase being used partly for increased melting of sea ice in summer, resulting in thinner ice in early winter, which then allows for a larger upward heat flux through the ice to the atmosphere and enhanced atmospheric warming in winter. Robock (1983) questioned this explanation on the basis of an EBCM having neither surface-air resolution nor explicit sea ice physics. Robock (1983) argued that the enhanced winter warming obtained in his model and in MS is a result of what he called a 'sea-ice thermal inertia feedback'. In Robock's model the effect of sea ice on model climate is parameterized in two ways: the first parameterization involves the well-known albedo feedback, and the second parameterization is to make the effective ocean thermal inertia dependent on the sea ice fraction. As the model climate warms in response to an increase in the

external forcing, the effective zonal thermal inertia increases, which reduces seasonal warming in summer and cooling in winter, resulting in greater model high latitude warming in winter than in summer. Since this pattern resembles that obtained by MS, Robock (1983) dismissed their explanation and instead claimed that his thermal inertia feedback was the explanation for the enhanced winter sensitivity in both his model and in the GCM of MS.

Robock's (1983) thermal inertia feedback, however, is merely an attempt to parameterize the effect of a whole series of physical process operating in the MS GCM but which are of necessity absent in his EBCM because of its lack of surface-air resolution. The EBCM used here, on the other hand, contains surface-air resolution and much of the same sea ice physics found in MS. In order to gain further insight into the mechanisms responsible for the seasonal pattern of temperature response obtained in models with explicit sea ice physics, experiments were performed using an alternative sea ice parameterization whereby an ocean zone is either entirely ice-free or entirely ice covered. This shall be referred to as the 'all-or-nothing' parameterization. With this parameterization complete ice cover persists year round poleward of 80° N and 65° S.

In analyzing model results, the following two quantities are computed: (1) the upward heat flux from the ocean to the atmosphere, averaged over the ice-free and ice-covered regions, and (2) convergence of oceanic meridional heat flux. Over ice-covered regions the upward heat flux is equal to the upward conductive heat flux within the ice plus the rate of release of the latent heat of fusion in the atmosphere associated with snowfall, minus the heat flux used for surface melting of ice or snow. Over the ice-free region it is given by the net surface radiation minus the upward turbulent heat fluxes plus the latent heat of fusion associated with snowfall. The oceanic meridional heat flux convergence consists of sensible heat flux convergence, a latent heat flux component associated with meridional advection of sea ice, and the prescribed upward heat flux F_b at the base of sea ice or of the ice-free mixed layer.

At equilibrium the mean annual ocean-air heat flux exactly balances the oceanic meridional heat flux convergence. In zones with year round ice cover the only component to the oceanic heat flux convergence is F_b, which leads directly to basal ice melting and keeps the ice thin enough that the upward heat flux to the atmosphere exactly balances this term in the annual mean.

When the solar constant is increased, the increased surface heating goes into increased melting of sea ice in summer in zones having sea ice, rather than increasing the surface temperature. At the start of winter the thinner ice results in a greater upward conductive heat flux within the ice, which leads to a warmer temperature at the ice-air interface and a corresponding increase in the upward ice-air heat flux. Associated with the greater upward heat flux is an increase in the rate of basal ice growth in winter following a climatic warming. With a 1% solar constant increase, for which sea ice still persists year round at 87.5° N, the upward ocean-air heat flux decreases by 23 W m^{-2} in June and increases by 11

W m^{-2} in September, with minimum and maximum atmospheric temperature responses of 0.4 °C in August and 3.6 °C in December. Thus, a strong seasonal variation of the change in ocean-air heat flux and associated atmospheric temperature response occurs in the absence of changes in ice extent, and solely as a result of changes in ice thickness. This behavior cannot be captured by parameterizing the thermal inertia in terms of zonal ice fraction.

Similarly, when the solar constant is decreased there is a strong seasonal variation of the change in ocean-air heat flux and temperature response, even in zones where the sea ice fraction does not change. Since, during the summer melt season, surface temperature is limited not by the external forcing but by the presence of ice, the surface temperature does not fall when the solar constant is decreased, although the rate of melting decreases. This causes the ice to be thicker at the start of winter, which results in less basal ice freezing in winter in spite of the colder air temperatures. For a 2% solar constant decrease this leads to an increase in the ocean-air heat flux of 30 W m^{-2} in June and a decrease of 11 W m^{-2} in October at 87.5° N.

Since the mean annual net ice budget is zero at equilibrium, the changes in summer surface melting and winter basal freezing following a solar constant change exactly cancel out in the annual mean. Furthermore, using the all-or-nothing parameterization, the large summer and winter changes in ocean-air heat flux also exactly cancel out in the annual mean in zones where there is no change in mean annual ice fraction. In effect, the change in external forcing is merely redistributed between summer and winter through compensating changes in summer surface melting and winter basal freezing. A change in the mean annual ocean-air heat flux occurs only in zones where there is a change in the mean annual sea ice fraction. Since, at equilibrium, the mean annual ocean-air heat flux is constrained to equal the mean annual oceanic meridional heat flux convergence, the changes in these two quantities are also equal. The feedback between ice extent and the mean annual ocean-air heat flux is thus dependent on the feedback between ice extent and meridional oceanic heat flux.

Thus, we can identify two separate effects of sea ice changes on the ocean-air heat flux operating through entirely different mechanisms: (1) changes in sea ice thickness which, acting alone, lead to a seasonal redistribution of the ocean-air flux with no change in the annual mean, and (2) changes in sea ice extent, which lead to a change in the mean annual ocean-air heat flux (as well as in the seasonal distribution), and are dependent on changes in the meridional oceanic heat flux convergence.

Figure 6 shows the change in seasonal ocean-air heat flux at 82.5° N and at 76.25° N for a 2% solar constant increase and decrease using the original sea ice model, in which partial and continuously varying sea ice fraction is permitted. The largest changes in the fall or winter occur in months with the largest change in ice extent, whereas the largest change in the spring or summer flux occurs in the month with the largest change in cumulative surface melt. Thus, the largest

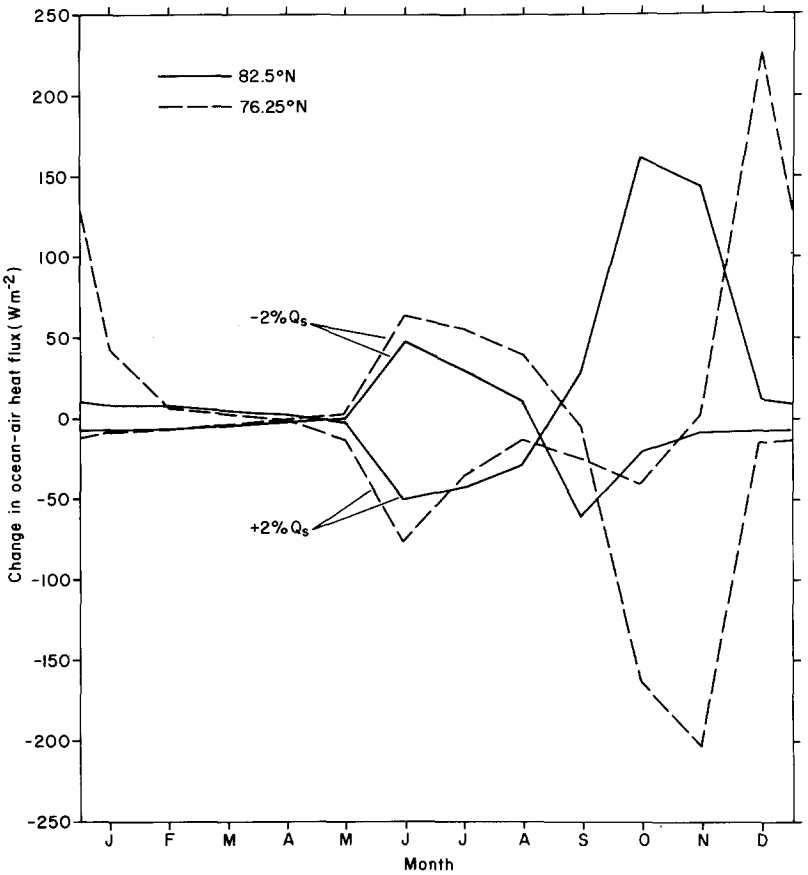

Fig. 6. Change in ocean-air heat flux at 82.5° N (solid lines) and at 76.25° N (dahsed lines) for a 2% solar constant decrease and a 2% solar constant increase.

summer change occurs in June at both latitudes and for either solar constant change, whereas the peak fall or winter change occurs later for a solar constant increase than for a decrease, and occurs progressively later at lower latitudes.

Figure 7 shows the latitudinal dependence of the change in mean annual ocean-air heat flux for a 2% solar constant decrease for the base case model version as well as for another experiment discussed below. Note that the regions of large decrease in mean annual ocean-air heat flux in the zones of increased sea ice fraction are compensated by a large increase in the ocean air heat flux equatorward of the sea ice limits. In equilibrium the global mean ocean-air heat flux is zero, so the global mean of the ocean-air heat flux changes shown in Figure 7 is zero.

Finally, note that since increases in both summer surface melting and winter basal freezing accompany an increase in the solar constant, the range of seasonal variation of sea ice thickness increases (by up to 30%) in zones where ice persists

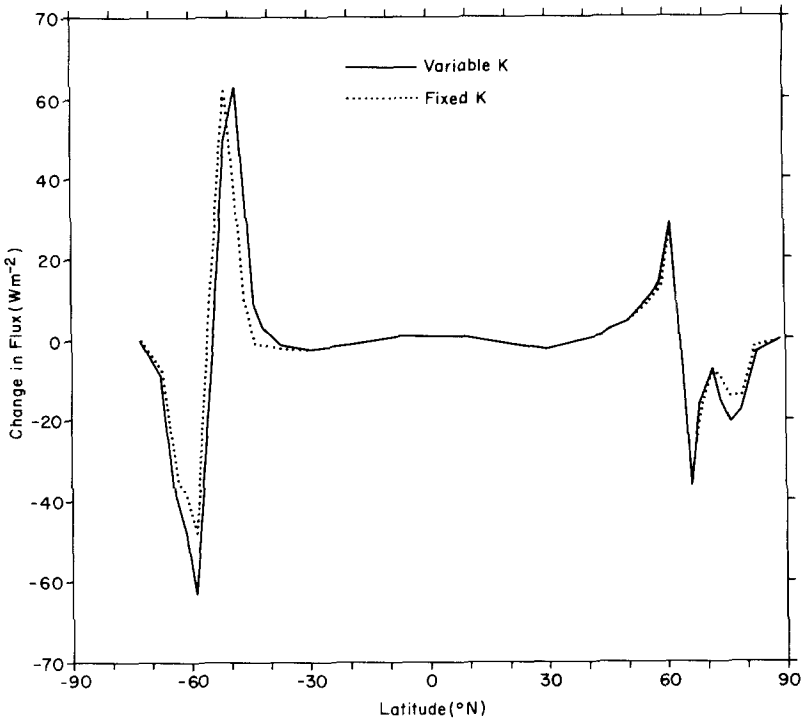

Fig. 7. Comparison of changes in mean annual ocean-air heat flux for a 2% solar constant decrease using fixed oceanic diffusion coefficients and diffusion coefficients scaled by the ice-free fraction.

year round. In the Antarctic region bottom water formation is largely dependent on the intensity of seasonal sea ice formation (Foster and Middleton, 1980). Thus, a potentially important link exists between climatic change, the seasonal variation of sea ice thickness, and bottom water formation.

4.3. *Role of Feedback Between Ice Area and Oceanic Meridional Heat Flux*

In the base case model version, presented above, the oceanic meridional diffusion coefficient for sensible heat is multiplied by the ice-free fraction at the end of each month, and operates on the meridional temperature gradient of the ice-free mixed layer. Thus, as the ice extent changes, the oceanic diffusion coefficient also changes. Johnson and Andrews (1979) suggested that changes in the ability of the ocean to transport heat poleward as a result of changes in sea ice extent could be an important feedback mechanism for high latitude temperature. In the present model, changes in sea ice extent affect meridional heat transport by changing both the oceanic diffusion coefficient and by leading to changes in the meridional ice-free mixed layer temperature gradient. To investigate the importance of the first effect, experiments were performed in which the solar constant is increased and decreased by 2%, but the monthly oceanic diffusion

TABLE VI: Comparison of mean annual, zonally averaged high latitude atmospheric temperature response to a 2% solar constant decrease and increase with fixed oceanic diffusion coefficients and with diffusion coefficients scaled by the ice free fraction, as in the base case model version.

	$-2\%\ Q_s$		$+2\%\ Q_s$	
Latitude	Fixed K_0	Variable K_0	Fixed K_0	Variable K_0
79° N	−4.53	−4.76	4.19	5.33
69° N	−4.45	−4.53	4.00	4.46
59° N	−3.52	−3.51	3.42	3.44
49° N	−3.35	−3.34	3.25	3.22
41° S	−3.38	−3.85	3.16	3.23
49° S	−4.07	−4.31	3.35	3.47
59° S	−5.48	−7.70	3.47	3.77
68° S	−6.95	−7.77	4.50	6.67
78° S	−5.97	−6.63	4.17	5.96

coefficients are held fixed at their unperturbed values. The high latitude mean annual, zonally averaged atmospheric temperature response to a 2% solar constant decrease and increase are compared for the fixed and variable oceanic diffusion coefficient cases in Table VI, while changes in mean annual oceanic meridional heat flux convergence (which is equal to the change in mean annual ocean-air heat flux in equilibrium) are compared for a solar constant decrease in Figure 7. In the Southern Hemisphere the temperature response is enhanced by up to 40% for a solar constant increase, but by no more than 25% for a solar constant decrease, while in the Northern Hemisphere the maximum zonal enhancements are 30% and 10%, respectively. These are zonal mean results and differ little between land and sea in the present model; nevertheless, one can expect local effects near regions of sea ice change to be greater.

Feedback between sea ice extent and meridional oceanic heat flux is thus seen to be a moderately important process, as suggested by Johnson and Andrews (1979), although it is of less importance for climatic cooling and is less relevant to the ice age problem than to cases of climatic warming. One must also keep in mind that simple diffusive oceanic heat transport is used here.

4.4. *Effect of Vegetational Masking*

This section examines the effect on model sensitivity of partial masking of snow-cover by vegetation as parameterized here, without taking into account possible shifts of the forest-tundra ecotone (which is fixed for the base case model version). Table I shows the land zonal fraction covered in tundra + polar desert, other non-forest vegetation, and forest vegetation, as used in the base case model version. The non-forest, non-tundra categories have roughnesses comparable to

that of tundra so that, when vegetational masking effects are parameterized using Equations (1) and (2), the vegetational masking is effective only in the forested part of the zone. Since OCA assumed all non-tundra or polar desert to be coniferous forest, the following three cases are considered here: (1) a case in which vegetational masking effects are computed assuming all non-tundra or polar desert regions to be coniferous forest, subsequently referred to as the coniferous forest case; (2) the base case; and (3) a case in which no vegetational masking effects are included. The mean annual, zonally averaged atmospheric temperature responses for these three cases are compared in Figure 8 for a 2% solar constant decrease and increase. Contributions of land snow cover changes to the globally averaged radiative forcing (ΔJ) are given in Table VII, and mean annual, Northern Hemisphere land and land + ocean atmospheric temperature responses are given in Table VIII. In Table IX the mean Northern Hemisphere atmospheric temperature responses obtained with the present model are compared with those obtained by OCA.

As seen from Figure 8, there is little difference in the absolute temperature responses between the base and coniferous forest cases. For a solar constant decrease, removal of vegetational masking enhances the absolute temperature

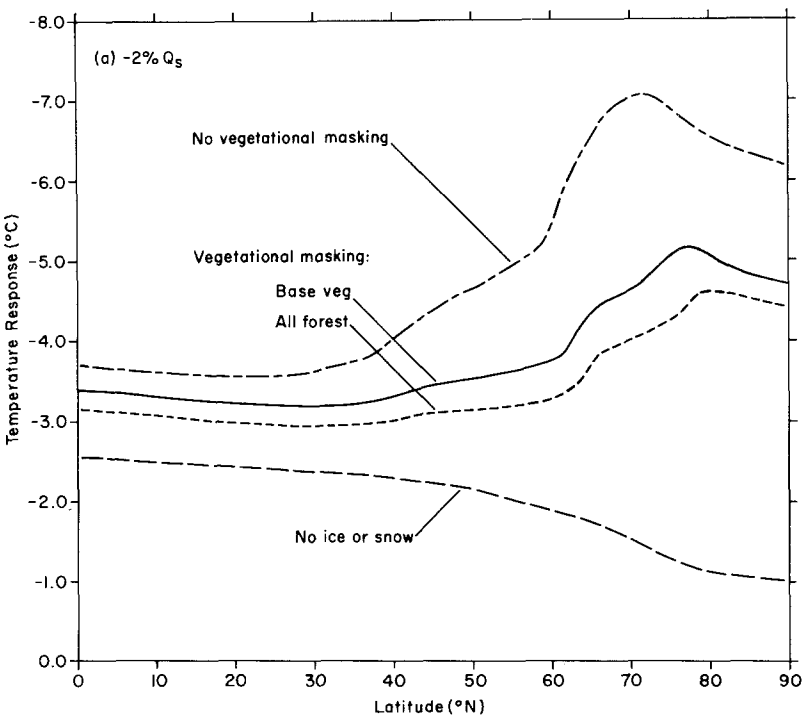

Fig. 8. Mean annual, zonally averaged atmospheric temperature response to (a) a 2% solar constant decrease, and (b) a 2% solar constant increase, for cases of no vegetational masking of snowcover, partial vegetational masking using the base case vegetation fractions, and partial vegetational masking assuming all non-tundra or non-polar desert to be coniferous forest.

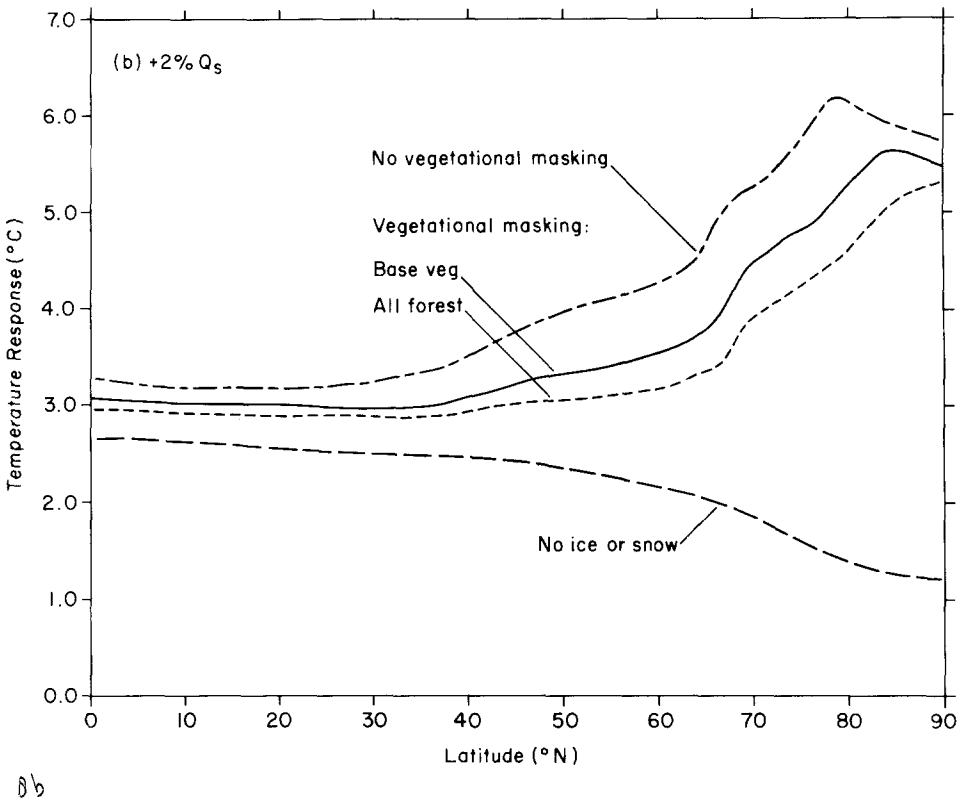

response by about 1/3 to 1/2, but by only 1/4 to 1/3 for a solar constant increase. Figure 8 also shows the temperature response obtained in the complete absence of snow and ice; comparing this response with the base case and no masking case, it can be seen that removal of vegetational masking roughly doubles the effect of ice and snow feedbacks on the zonally averaged temperature response at most latitudes.

Removal of vegetational effects enhances the hemispheric mean temperature response by about 30% and 20% for a solar constant decrease and increase, respectively, compared to the coniferous forest case (Table VIII). Using the base case vegetation fractions, these enhancements are reduced to only 20% and less than 10%, respectively. These enhancements are small compared to the relative differences in the radiative forcing change caused by changes in land snowcover (Table VII) because the absolute differences in snowcover radiative forcing with and without vegetational masking are quite small compared to the total radiative forcing change resulting from internal feedbacks (Table III).

OCA found that removal of vegetational masking effects enhanced the hemispheric mean temperature response by 62% and 25% for a 2% solar constant decrease and increase, respectively, which is considerably greater than obtained here. The greater sensitivity to vegetational masking obtained by OCA

is most likely a result of their use of a mean annual model rather than a seasonal model. In the model used here, land snow completely disappears during at least part of the summer, resulting in a smaller snow feedback and smaller sensitivity to vegetational masking than if the mean annual snow fraction change were applied to the mean annual insolation.

4.5. *Effect of Forest-Tundra Ecotone Shifts*

In this section the effect on model sensitivity of parameterizing the tundra fraction using Equations (4) and (5) is investigated. Figure 9 shows the change in tundra fraction following a 2% solar constant decrease and increase when the

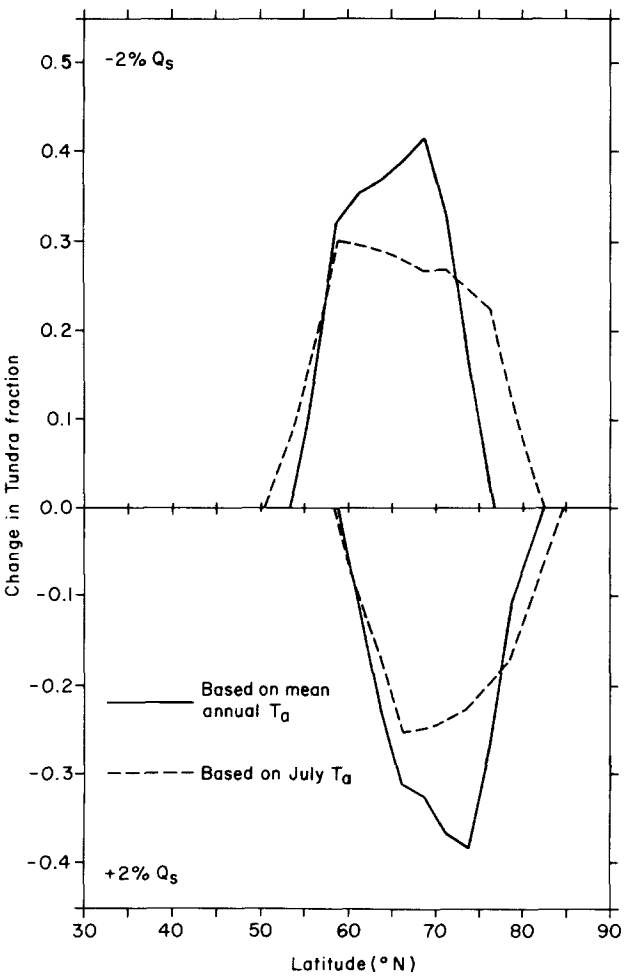

Fig. 9. Change in tundra fraction for a 2% solar constant decrease and increase when the tundra fraction is parameterized as a function of either mean annual land air temperature or July land air temperature. Base case non-tundra vegetation categories are used.

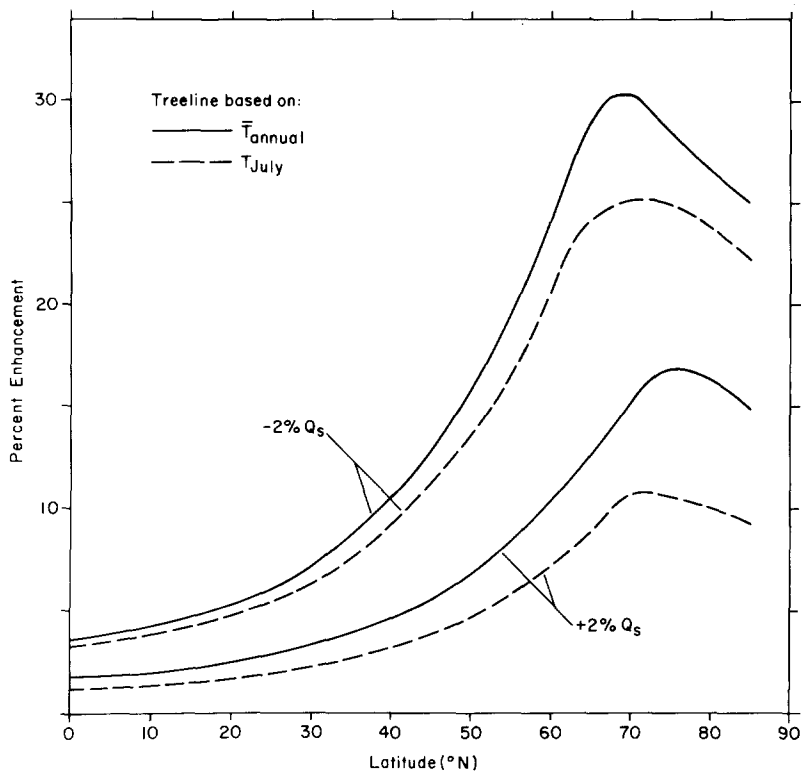

Fig. 10. Percent enhancement of the mean annual atmospheric temperature response over land for a 2% solar constant decrease and increase when the tundra fraction is parameterized as a function of either mean annual land air temperature or July land air temperature. Base case non-tundra vegetation categories are used.

tundra fraction is parameterized either in terms of mean annual or July land air temperature, and Figure 10 shows the resulting percentage enhancement of the mean annual land air temperature response. When the tundra fraction is allowed to vary, the relative proportions of the other vegetation types are held fixed; assuming all the non-tundra vegetation to be coniferous forest (as in OCA) increases the enhancement by only 1–3%.

As expected, the enhancement is smaller using the July tundra parameterization. Like OCA, allowing the tundra-forest ecotone to shift with climate has a greater effect on climate sensitivity to a solar constant decrease than to an increase. However, the effect obtained here is considerably smaller than obtained by OCA, who obtained maximum enhancements about three times larger than obtained here for both a 2% solar constant decrease and increase. In Table IX the enhancement of the mean annual Northern Hemisphere temperature response (averaged over land and sea) with a shifting tundra-forest ecotone is compared for the present model and as obtained by OCA. For a 2% solar constant increase, the hemispheric mean enhancement obtained here is about

TABLE VII: Globally averaged radiative forcing (ΔJ_i, W m^{-2}) from Northern Hemisphere land snow cover changes (not in parenthesis) and sea ice changes (in parenthesis) for the same experiments as shown in Figure 8.

Case	−2% Q_s		+2% Q_s	
Coniferous	−0.080	(−0.142)	0.084	(0.135)
Base	−0.196	(−0.153)	0.163	(0.139)
No vegetational masking	−0.702	(−0.394)	0.514	(0.224)

TABLE VIII: Comparison of Northern Hemisphere land and ocean + land mean annual atmospheric temperature responses (°C) to a 2% solar constant decrease and increase for the same experiments as shown in Figure 8.

Case	−2% Q_s		+2% Q_s	
	Land	Mean	Land	Mean
Coniferous	−3.25	−3.23	3.20	3.17
Base	−3.38	−3.32	3.30	3.24
No vegetational masking	−4.25	−3.99	3.82	3.65

TABLE IX: Comparison of mean annual, Northern Hemisphere atmospheric temperature responses obtained with the present model and by Otterman *et al.* (1984). High α refers to the case without partial vegetational masking of snowcover. Annual shift and July shift refer to tundra fraction parameterizations based on mean annual and July land air temperatures, respectively. Values in parenthesis under these columns are the amounts by which the temperature response is enhanced compared to cases in which the tundra fraction is freely parameterized for the present solar constant, then held fixed.

Model	Fixed ecotone		Shifting ecotone	
	High α	Low α	Annual shift	July shift
−2% Q_s				
Present	−3.99	−3.23	−3.65 (−0.33)	−3.58 (−0.28)
OCA	−4.32	−2.67	−3.73 (−1.06)	–
+2% Q_s				
Present	3.65	3.17	3.39 (0.18)	3.30 (0.11)
OCA	3.47	2.77	3.05 (0.28)	–

half that obtained by OCA using the mean annual parameterization, and about one third that obtained by OCA using the July temperature parameterization, but only 1/4 to 1/3 that obtained by OCA for a 2% solar constant decrease.

Figure 11 shows the mean annual change in radiative forcing averaged over

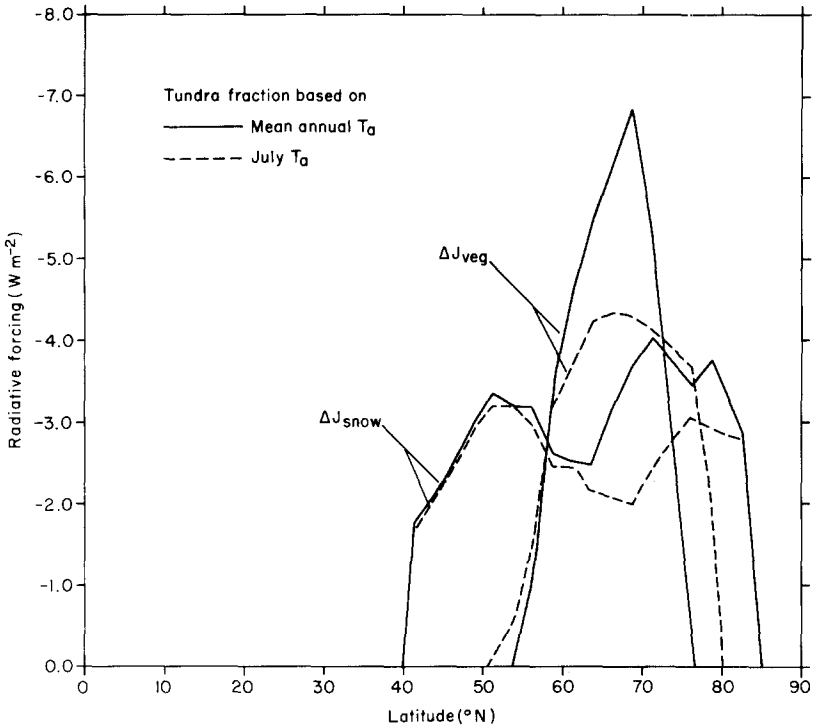

Fig. 11. Mean annual change in radiative forcing (ΔJ) over land caused by vegetation and snow cover changes acting alone for a 2% solar constant decrease when the tundra fraction is parameterized as a function of either mean annual land air temperature or July land air temperature. Base case non-tundra vegetation categories are used.

land, ΔJ_{veg} and ΔJ_{snow}, resulting from the equilibrium changes in vegetation fraction and in snow cover acting alone for both tundra parameterizations for a 2% solar constant decrease. Locally, ΔJ_{veg} exceeds ΔJ_{snow} by as much as 50% using the mean annual parameterization, and by as much as 100% using the July parameterization; in the former case, peak mean annual ΔJ_{veg} values of over 6

TABLE X: Comparison of globally averaged change in radiative forcing (ΔJ) caused by changes in vegetation fraction and land snow cover acting alone for a 2% solar constant decrease and increase, for the base case (having fixed vegetation) and cases in which the tundra fraction is parameterized in terms of the mean annual and July land air temperature.

Case	ΔJ_{veg}		ΔJ_{snow}	
	−2% Q_s	+2% Q_s	−2% Q_s	+2% Q_s
Base case	0.000	0.000	−0.211	0.180
July	−0.162	0.090	−0.230	0.153
Mean annual	−0.181	0.143	−0.272	0.188

W m^{-2} occur, compared to peak ΔJ_{snow} values of only 4 W m^{-2}. In Table X the globally averaged values of ΔJ_{veg} and ΔJ_{snow} are given for both tundra parameterizations and for both a solar constant decrease and increase.[2] Also shown is ΔJ_{snow} for the base case. Globally, ΔJ_{veg} is about one third smaller than ΔJ_{snow}, and the two are thus comparable in magnitude. As with the difference between ΔJ_{snow} with and without vegetational masking discussed in the previous section, ΔJ_{veg} and ΔJ_{snow} are both small compared to the radiative forcing changes resulting from other model feedbacks. In particular, the high latitude land temperature response is largely governed by the high latitude ocean response and hence by sea ice feedbacks, as may be inferred from the fact that the maximum land temperature response occurs in Winter (Figure 2) even though the maximum radiative forcing change resulting from vegetation and snowcover changes occurs in late Spring. This explains why a shifting treeline has relatively little effect on land temperature response in the present model.[3]

In a final set of treeline experiments, the effect of using the tundra parameterization based on mean annual air temperature and the OCA parameterization was tested in a mean annual version of the model (OCA used a mean annual model). In this case a maximum enhancement of the zonal land temperature response of 80% occurs using the OCA parameterization, with an enhancement in the Northern Hemisphere mean temperature response by 1.0 °C – both comparable to that obtained by OCA. Using the parameterization presented here, on the other hand, the enhancements are only half as large, but still larger than obtained in the seasonal model version. However, an analysis of the ΔJ_i's and the associated feedback factors for vegetation, ice, and snow indicates that the primary cause of the much greater sensitivity to vegetational shifts using the OCA parameterization in the mean annual model version is that the strengths of the ice and snow feedbacks themselves (as represented by f_{ice} and f_{snow}) are greater for this case, rather than being largely a result of stronger vegetational feedback.

[2] As a check on the linearity assumption underlying the ΔJ_{veg} and ΔJ_{snow} values shown in Figure 11 and in Table X, the same residual error as shown for the ΔJ_i column in Table III were computed for each of the experiments shown in Table X, and were all less than 0.03 W m^{-2} in magnitude.

[3] The above experiments also serve to illustrate a weakness of the linear feedback analysis methodology used here. Using the data in Tables IX and X for the 2% solar constant decrease experiment with a shifting ecotone based on the mean annual temperature, one can calculate an f_{veg} of 0.015 and a total f of 0.648. From Equation (10) one expects a reduction in ΔT when f_{veg} is subtracted from f of 0.16 °C, whereas the actual reduction is 0.36 °C. This discrepancy implies that the feedback factors associated with other processes have in fact changed with the removal of vegetational feedback, which is contrary to our assumption that the individual f_i are constant as further feedback processes are added. The ΔJ_i computed for individual feedback processes do nevertheless accurately reflect the relative contributions to the total response of each process for the particular experiment in question, as indicated by the small residuals noted above. Caution is required, however, when using the f_i computed from the ΔJ_i to estimate what the model response would be in the absence of a given feedback process.

4.6. *Role of Surface Albedo Temperature Dependence*

In the final expriments presented here the importance to model sensitivity of the directly parameterized dependence of ice and snow albedo on temperature is investigated. In Figure 12 the contribution to the mean annual, zonally averaged $\Delta J_{\text{snow}} + \Delta J_{\text{ice}}$ with and without changes in snow and ice albedos included are compared for the Northern Hemisphere. It can be seen that changes in snow and ice albedo make an important contribution to $\Delta J_{\text{snow}} + \Delta J_{\text{ice}}$ poleward of 70° N only. The difference in global mean $\Delta J_{\text{snow}} + \Delta J_{\text{ice}}$ is only 0.054 W m^{-2}, which gives a feedback factor of 0.004 and, in its absence, would lead to a difference in global mean temperature response of only 0.038 °C based on Equation (10). To determine the local effect on temperature of the snow and ice albedo contribution to $\Delta J_{\text{snow}} + \Delta J_{\text{ice}}$, the snow and sea ice albedos computed at each time step once the model reached equilibrium with the present solar constant were stored and applied at corresponding time steps in the seasonal cycle once a solar constant increase was applied. Maximum mean annual, zonally averaged

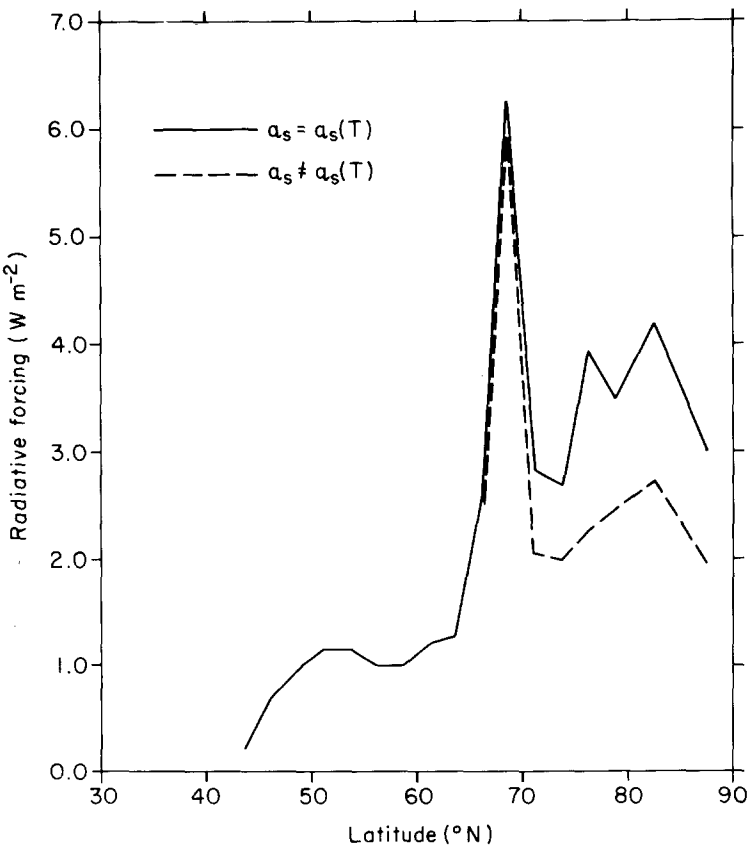

Fig. 12. Effect of parameterized surface albedo temperature dependence on the mean annual radiative forcing change cuased by changes in ice and snow.

temperature differences of only 0.2 °C occurred, and the global mean temperature response was reduced by 0.039 °C, in close agreement with the above analysis.

To understand why the parameterized snow and ice albedo temperature dependence has such a small effect on ΔJ_{snow} and hence on model sensitivity, recall that parameterized temperature effects for sea ice albedo occur only between temperatures of −3 °C and 0 °C. During the summer melting period, when insolation is high, sea ice albedos are at their minimum values. With fixed albedos following a solar constant increase the seasonally varying albedos are locked at their previous seasonal values. With freely predicted albedos, however, the transition from seasonally high to seasonally low albedos merely occurs one or two time steps sooner (6 day time steps are used) so that, averaged over the year, there is little change in absorbed solar energy. Thus it can be concluded that, all else being equal, the parameterized temperature dependence of the ice and snow albedo has very little effect on model sensitivity to external forcing changes.

As shown in Harvey (1988a), the albedo temperature dependence does have a significant effect on both equilibrium sea ice extent and thickness for the present external forcing. These differences make it difficult to assess the importance of the albedo temperature dependence to sensitivity if experiments are compared with the dependence present for both the present and increased solar constant, and absent altogether. This approach was used by Washington and Meehl (1986; henceforth referred to as WM) in a mean annual model, who obtained globally averaged surface air temperature response for CO_2 doubling of 1.3 °C with fixed ice and snow albedos, and 1.6 °C with temperature-dependent albedos.

Using the same approach in the present model gives a greater sensitivity (by about 0.1 °C) for the variable albedo case using the mean annual version but not with the seasonal version. Part of the problem is that the starting climates are different for the fixed and variable albedo cases. Spelman and Manabe's (1984) results indicate that a minimum condition for meaningfully comparing model sensitivities to an external forcing change is that they have comparable starting ice and snow areas. However, if the solar constant is increased for the fixed albedo case to give identical initial starting ice areas for the fixed and variable albedo cases, the global mean temperature for the fixed albedo case is 0.7 °C warmer. As a consequence the global mean water vapor feedback is stronger for the fixed albedo case, which tends to give it a greater sensitivity than the variable albedo case.

The above experiments illustrate the great difficulty in estimating the importance of a given feedback process when addition of that process results in different starting climates. In the present model it is possible, by adjusting the solar constant, to obtain the same globally averaged starting temperature or starting ice area for experiments with different albedo parameterizations, but not both. Because it is not possible to simultaneously match all the climate param-

eters which influence model sensitivity, it is possible for the addition of a given process to have a qualitatively different effect in mean annual and seasonal versions of the same model. The best way around these difficulties seems to be to run a model with a given feedback process present and to calculate the corresponding ΔJ_i. As we have seen, the calculated ΔJ_i accurately reflect the relative contributions to the total response of the feedback processes considered here (although problems can arise with some cloud properties, as discussed in Schlesinger, 1985), and the global mean effect of removing a given process can be computed from Equation (10) under the assumption that the strengths of all the other processes (as measured by the f_i) do not change. Even though this assumption may not be strictly valid it is nevertheless useful, within the context of a given experiment with multiple feedback processes, to know what would happen if it were valid and a given process were to be removed.

5. Discussion and Conclusions

A seasonal energy balance climate model has been used to investigate and clarify the roles of high latitude ice, snow, and vegetation feedback processes. Sea ice feedback is found to have a 5–8 times greater effect on the global mean radiative balance than land snow cover feedback, and to be more important in the Southern Hemisphere than in the Northern Hemisphere, leading to a greater Southern Hemisphere sensitivity to solar constant variations. Both the greater importance of sea ice feedback and the greater sensitivity of the Southern Hemisphere are contrary to commonly held assumptions. Increased winter cooling will lead to a land snow cover feedback in summer only if sufficient snow falls to survive summer melting. The sea ice feedback, on the other hand, is not limited by the hydrological cycle; colder winters lead to thicker ice which is harder to melt in the summer whether or not snowfall increases. Snow cover feedback is also limited in reality as well as in the present model by the masking effect of vegetation. Thus, although the quantitative results obtained with this or any other EBCM should not be taken literally, the qualitative results concerning the importance of sea ice feedback are credible.

The separate contributions of changes in ice thickness and in ice extent to changes in the mean annual ocean-air heat flux have been isolated and shown to be poorly represented by a 'sea-ice thermal inertia feedback'. Changes in ice thickness acting alone lead to compensating changes in summer surface melting and winter basal freezing, with no change in the mean annual upward ocean-air heat flux. Changes in the mean annual ocean-air heat flux require changes in mean annual ice extent and are dependent on the feedback between ice extent and meridional oceanic heat flux. This is because, in equilibrium, the mean annual change in ocean-air heat flux in a given zone is constrained to equal the mean annual change in meridional oceanic heat flux convergence.

The effect of partial masking of snowcover by forests, and of shifts in the

tundra-forest ecotone, is found to be considerably smaller in the present model than that obtained by Otterman *et al.* (1984), particularly if the tundra fraction is parameterized in terms of July land air temperature rather than in terms of mean annual land air temperature. Similarly, the parameterized temperature dependence of ice and snow albedos is found to be significantly less important to climate sensitivity than indicated by Washington and Meehl (1986). In both cases, the sensitivity of these models is higher in part because they are mean annual rather than seasonal models.

The linear feedback analysis methodology adopted here is a convenient tool for quantifying and comparing feedback processes. In particular, by computing radiative forcing changes, ΔJ_i, associated with individual feedback processes, the direct effect on the temperature response can be computed as $G_0 \Delta J_i$, whereas the net effect of removing a given process can be computed using the associated feedback factor, f_i, under the assumption that the strengths of all the other processes do not change.

Acknowledgment

This research was supported by Natural Sciences and Engineering Research Council of Canada grant No. A1413, and was performed using the Ontario Centre for Large Scale Computation Cray-XMP/22.

References

Briegleb, B. and Ramanathan, V.: 1982, 'Spectral and Diurnal Variations in Clear Sky Planetary Albedo', *J. Appl. Meteor.* **21**, 1160–1171.

Crutcher, H. L. and Meserve, J. M., 1970: *Selected Level Heights, Temperatures, and Dew Points for the Northern Hemisphere*, NAVAIR 50-1C-52, Chief Nav. Op., Washington.

Dickinson, R. E., Meehl, G. A., and Washington, W. M., 1987: 'Ice-albedo Feedback in a CO_2-doubling Simulation', *Clim. Change* **10**, 241–248.

Foster, T. D. and Middleton, J. H.: 1980, 'Bottom Water Formation in the Western Weddell Sea', *Deep Sea Res.* **27A**, 367–381.

Hare, F. K. and Hay, J. E.: 1974, 'The Climate of Canada and Alaska', in Bryson, R. A. and Hare, F. K. (eds.), *The Climates of North America, World Survey of Climatology, Vol. 11*, Elsevier, pp. 49–192.

Harvey, L. D. D.: 1988a, 'A Semi-analytic Energy Balance Climate Model with Explicit Sea Ice and Snow Physics', *J. Clim.* (in press).

Harvey, L. D. D.: 1988b, 'Development of a Sea Ice Model for Use in Zonally Averaged Energy Balance Climate Models', *J. Clim.* (in press).

Harvey, L. D. D.: 1988c, 'Milankovitch Theory, Interhemispheric Differences in Climate Sensitivity, and North Atlantic Bottom Water Formation', (in prep.).

Hibler, W. D.: 1980, 'Modeling a Variable Thickness Sea Ice Cover', *Mon. Wea. Rev.* **108**, 1943–1973.

Imbrie, J. and Imbrie, J. Z.: 1980, 'Modeling the Climatic Response to Orbital Variations', *Science* **207**, 943–953.

Johnson, R. G. and Andrews, J. T.: 1979, 'Rapid Ice-sheet Growth and Initiation of the Last Glaciation', *Quat. Res.* **12**, 119–134.

Manabe, S. and Stouffer, R. J.: 1980, 'Sensitivity of a Global Climate Model to an Increase of CO_2 Concentration in the Atmosphere', *J. Geophys. Res.* **85**, 5529–5554.

Manabe, S. and Wetherald, R. T.: 1967, 'Thermal Equilibrium of the Atmosphere with a Given Distribution of Relative Humidity', *J. Atmos. Sci.* **24**, 241–259.

Mercer, J. H.: 1984, 'Simultaneous Climatic Change in Both Hemispheres and Similar Bipolar Interglacial Warming: Evidence and Implications', in Hansen, J. E., and Takahashi, T. (eds.), *Climate Processes and Climate Sensitivity* (Maurice Ewing Series, No. 5), American Geophysical Union, Washington, pp. 307–313.

Milankovitch, M. M.: 1941, *Canon of Insolation and the Ice Age Problem*, Beograd, Koniglich Serbische Akademie. English translation by the Israel Program for Scientific Translations, published for the National Science Foundation, Washington, D.C. (1969).

Otterman, J., Chou, M.-D., and Arking, A.: 1984, 'Effects of Nontropical Forest Cover on Climate', *J. Clim. Applied Meteor.* **23**, 762–767.

Parkinson, C. L. and Washington, W. M.: 1979, 'A Large-Scale Numerical Model of Sea Ice', *J. Geophys. Res.* **84**, 311–337.

Pollard, D.: 1983, 'A Coupled Climate-Ice Sheet Model Applied to the Quaternary Ice Ages', *J. Geophys. Res.* **88**, 7705–7718.

Robock, A.: 1983, 'Ice and Snow Feedbacks and the Latitudinal and Seasonal Distribution of Climate Sensitivity', *J. Atmos. Sci.* **40**, 986–997.

Schlesinger, M. E.: 1985, 'Analysis of Results from Energy Balance and Radiative-convective Models', in MacCracken, M. C. and Luther, F. M. (eds.), *Projecting the Climatic Effects of Increasing Carbon Dioxide*, U.S. Dept. Energy, DOE/ER-0237, Washington, pp. 281–319.

Schlesinger, M. E. and Mitchell, J. F. B.: 1985, 'Model Projections of the Equilibrium Climatic Response to Increased Carbon Dioxide', in MacCracken, M. C. and Luther, F. M. (eds.), *Projecting the Climatic Effects of Increasing Carbon Dioxide*, U.S. Dept. Energy, DOE/ER-0237, Washington, pp. 81–147.

Semtner, A. J.: 1976, 'A Model for the Thermodynamic Growth of Sea Ice in Numerical Investigations of Climate', *J. Phys. Oceanogr.* **6**, 379–389.

Short, D. A., North, G. R., Bless, T. D., and Smith, G. L.: 1984, 'Infrared Parameterization and Simple Climate Models', *J. Clim. Applied Meteor.* **23**, 1222–1233.

Spelman, M. J. and Manabe, S.: 1984, 'Influence of Oceanic Heat Transport upon the Sensitivity of a Model Climate', *J. Geophys. Res.* **89**, 571–586.

Thompson, S. L. and Warren, S. G.: 1982, 'Parameterization of Outgoing Infrared Radiation Derived from Detailed Radiative Calculations', *J. Atmos. Sci.* **39**, 2667–2680.

Washington, W. M. and Meehl, G. A.: 1986, 'General Circulation Model CO_2 Sensitivity Experiments: Snow-Sea Ice Albedo Parameterization and Globally Averaged Surface Air Temperature', *Clim. Change* **8**, 231–241.

(Received 19 August, 1987; in revised form 25 March, 1988)